

## Clouds and trace gas distributions during TRACE-P

J. Crawford,<sup>1</sup> J. Olson,<sup>1</sup> D. Davis,<sup>2</sup> G. Chen,<sup>2,3</sup> J. Barrick,<sup>1</sup> R. Shetter,<sup>4</sup> B. Lefer,<sup>4</sup>  
 C. Jordan,<sup>1</sup> B. Anderson,<sup>1</sup> A. Clarke,<sup>5</sup> G. Sachse,<sup>1</sup> D. Blake,<sup>6</sup> H. Singh,<sup>7</sup> S. Sandolm,<sup>2</sup>  
 D. Tan,<sup>2</sup> Y. Kondo,<sup>8</sup> M. Avery,<sup>1</sup> F. Flocke,<sup>4</sup> F. Eisele,<sup>4</sup> L. Mauldin,<sup>4</sup> M. Zondlo,<sup>4,9</sup>  
 W. Brune,<sup>10</sup> H. Harder,<sup>10,11</sup> M. Martinez,<sup>10,11</sup> R. Talbot,<sup>12</sup> A. Bandy,<sup>13</sup>  
 and D. Thornton<sup>13</sup>

Received 15 November 2002; revised 26 March 2003; accepted 17 April 2003; published 4 November 2003.

[1] This paper addresses the question: To what extent do trace gas distributions correspond to cloudiness? Observations taken during NASA's TRACE-P experiment indicate that there can be statistically significant differences in trace gas concentrations between clear-sky and cloudy areas. During the TRACE-P mission, frontal outflow of Asian emissions from the Pacific Rim to the western, North Pacific was sampled by NASA's DC-8 and P-3B aircraft. On several occasions, enhanced CO mixing ratios were observed in and around frontal clouds. A more detailed analysis of trace gas distributions revealed CO enhancements of 30% in the lower free troposphere (1–5 km) for cloudy regions as compared to clear areas. These enhancements exist within clouds as well as above and below clouds. In the upper free troposphere (5–11 km), overall enhancement in CO of 15% was observed although enhancements are mainly restricted to observations within clouds. These in-cloud observations were enhanced by factors of 1.5 to 2 over clear air data. Similar enhancements were seen for many other anthropogenic tracers. By contrast, distributions for O<sub>3</sub> revealed no clear differences between cloudy and clear regions suggesting that other influences (e.g., stratosphere-troposphere exchange) might complicate any correspondence with local cloudiness. Expected cloud influences on oxidation chemistry were evident in enhanced OH concentrations above clouds and depressed OH below clouds. These findings are particularly relevant to current and future satellite investigations of the troposphere. Understanding the potential biases created by the inability to probe cloudy regions will improve the interpretation of regional and globally averaged satellite observations. *INDEX TERMS:* 0365 Atmospheric Composition and Structure: Troposphere—composition and chemistry; 0368 Atmospheric Composition and Structure: Troposphere—constituent transport and chemistry; 0399 Atmospheric Composition and Structure: General or miscellaneous; *KEYWORDS:* troposphere, cloud, chemistry, transport, carbon monoxide, TRACE-P

**Citation:** Crawford, J., et al., Clouds and trace gas distributions during TRACE-P, *J. Geophys. Res.*, 108(D21), 8818, doi:10.1029/2002JD003177, 2003.

### 1. Introduction

[2] NASA's airborne field program known as the Global Tropospheric Experiment (GTE) was conceived as a focused research program with the goal of improving our understanding of global trace gas distributions and key

chemical cycles in the troposphere [McNeal *et al.*, 1983]. The core of the program was based on in situ sampling from aircraft supported by modeling and laboratory studies. Part of the vision behind these activities was the belief that they would provide the knowledge base critical to the planning, interpretation, and validation of future satellite based investigations of tropospheric chemistry. During NASA's

<sup>1</sup>NASA Langley Research Center, Hampton, Virginia, USA.

<sup>2</sup>School of Earth and Atmospheric Sciences, Georgia Institute of Technology, Atlanta, Georgia, USA.

<sup>3</sup>Now at NASA Langley Research Center, Hampton, Virginia, USA.

<sup>4</sup>Atmospheric Chemistry Division, National Center for Atmospheric Research, Boulder, Colorado, USA.

<sup>5</sup>School of Ocean and Earth Science and Technology, University of Hawaii, Honolulu, Hawaii, USA.

<sup>6</sup>Department of Chemistry, University of California, Irvine, California, USA.

<sup>7</sup>NASA Ames Research Center, Moffett Field, California, USA.

<sup>8</sup>Research Center for Advanced Science and Technology, University of Tokyo, Tokyo, Japan.

<sup>9</sup>Now at Southwest Sciences Inc., Santa Fe, New Mexico, USA.

<sup>10</sup>Department of Meteorology, Pennsylvania State University, University Park, Pennsylvania, USA.

<sup>11</sup>Now at Atmospheric Chemistry Department, Max Planck Institute for Chemistry, Mainz, Germany.

<sup>12</sup>Institute for the Study of Earth, Oceans, and Space, University of New Hampshire, Durham, New Hampshire, USA.

<sup>13</sup>Department of Chemistry, Drexel University, Philadelphia, Pennsylvania, USA.

TRACE-P (Transport and Chemical Evolution over the Pacific) campaign, GTE flight operations to support satellite validation were conducted for the first time [Jacob *et al.*, 2003]. Specifically, airborne sampling was planned to coincide in time and location with observations of CO by the MOPITT instrument. While these simultaneous observations constitute an important part of the link between aircraft and satellite observations, it is critical to examine the broader airborne data set for information that might be of interest to space-based observers. One useful piece of information relates to differences in trace gas observations for areas expected to be visible to these observing platforms versus those areas that will be obscured, specifically cloudy regions.

[3] Examining trace gas distributions in relation to local cloudiness is also relevant to improving our understanding of trace gas transport and photochemical evolution which was the primary objective of TRACE-P. The radiative impact of clouds serves to enhance photochemical oxidation chemistry above clouds through the backscattering of UV radiation [Thompson, 1984; Madronich, 1987; Junkermann *et al.*, 2002]. Conversely, the attenuation of radiation below clouds can slow photochemical processing, thus lengthening the lifetime of photochemically sensitive species and thereby increasing the range over which they can be transported. Heterogeneous processes (e.g., uptake of soluble species) within clouds can also exert an important influence on tropospheric composition.

[4] Despite the temporal and spatial limitations of airborne data, in situ sampling from airborne platforms remains to be the most effective way to gain detailed information about atmospheric composition in and around clouds. Examples of airborne data demonstrating the role of clouds in redistributing trace gases can be found in the literature [e.g., Dickerson *et al.*, 1987; Pickering *et al.*, 1996; Huntreiser *et al.*, 1998]. While these types of observations provide strong anecdotal evidence for a relationship between clouds and trace gas distributions, there have been no attempts to ascertain large-scale trends in trace gases with cloudiness through the statistical evaluation of larger, regional data sets.

[5] The TRACE-P mission was conducted during the spring of 2001 (24 February to 10 April) over the western, North Pacific along the Asian Pacific Rim. Two aircraft, NASA's DC-8 and P-3B, collected observations of an extensive suite of trace gases, most of which were measured on both aircraft (for details, see Jacob *et al.* [2003]). It is during this season that Asian outflow to the Pacific is maximized with frontal passages being a major influence on the outflow [Yienger *et al.*, 2000; Kaneyasu *et al.*, 2000; Bey *et al.*, 2001; Liu *et al.*, 2003]. The importance of frontal dynamics to trace gas distributions has also been investigated recently for the North Atlantic [Cooper *et al.*, 2002a, 2002b]. During TRACE-P, sampling in regions of frontally induced cloudiness frequently exhibited elevated trace gas mixing ratios.

## 2. Examples of Trace Gas Enhancements in Cloudy Regions

[6] On March 7, 2001 both aircraft profiled through a frontal cloud band. Figure 1 shows a satellite image of the

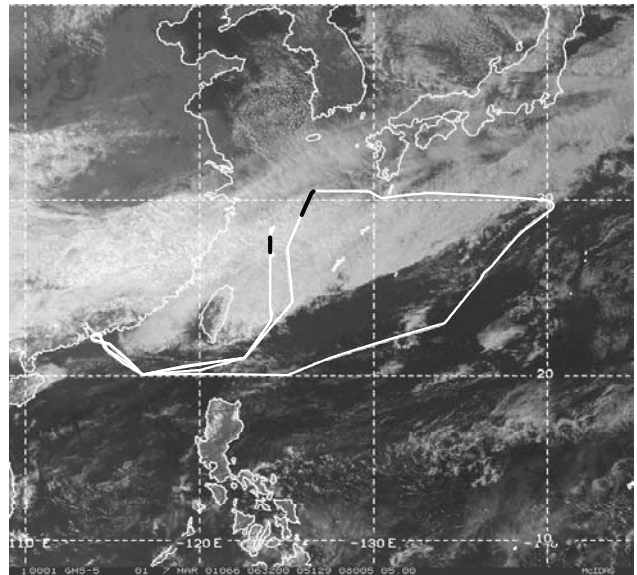


**Figure 1.** Visible imagery from the GMS satellite for 0632 UTC 7 March 2001. Flight tracks are overlaid for the P-3B and DC-8. The P-3B flight track is to the east of the DC-8 path. Locations of vertical profiles through frontal cloud for each aircraft are highlighted in black.

frontal cloud band overlaid with the flight tracks of the DC-8 and P-3B. The locations of profiles through the cloud band are further highlighted. Measurements of CO and relative humidity during these profiles are shown in Figure 2. Both the DC-8 and P-3B profiles show a layer of elevated CO (>300 ppbv). Relative humidity values show saturated conditions for the elevated CO layers. In-flight video during these two profiles further corroborates that these enhancements were measured within cloud.

[7] Although sampled at distinctly different locations and altitudes, observations exhibit enhancements of similar magnitude for the two aircraft. An apparent connection between the P-3B and DC-8 observations emerges when these profiles are compared using coordinates of equivalent potential temperature (Figure 3). The overlap suggests that the two aircraft sampled a single outflow feature of considerable geographic extent. The physical separation between the profiles was roughly 420 km, although the P-3B profile occurred 2 hours later and upwind of the DC-8 observation. Taking this temporal separation into account along with a P-3B measured wind speed of 30 m/s and wind direction of 250E, the actual separation between these two profiles is estimated to be about 650 km. One should not infer from this example that enhancements were observed for all cloud penetrations; however, distinct CO enhancement within clouds was observed on flights 11, 15, and 19 for the P-3B as well as flights 9, 13, 15, and 18 for the DC-8.

[8] It is important to note that enhancements in CO were not limited to in-cloud data. Synoptic-scale, shallow convection associated with frontal passages induces regional cloudiness, but the large-scale lifting of emissions impacts clear air as well. For instance, P-3B Flight 19 logged 5 hours of flight in the free troposphere between 1 and 5.5 km. During this time, a combined 47 minutes of enhanced CO in

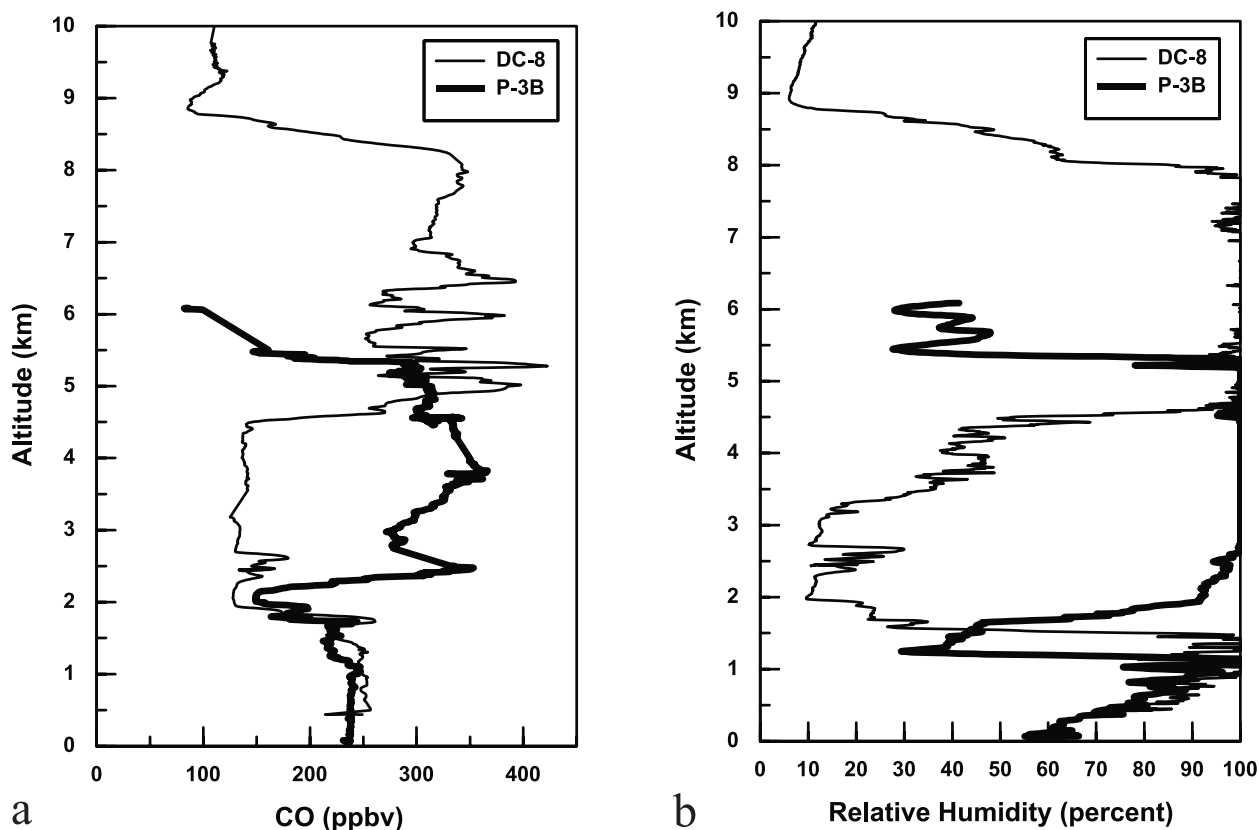


**Figure 2.** Vertical profiles of (a) CO and (b) relative humidity through frontal clouds on 7 March 2001.

the 300–500 ppbv range were sampled (average CO of  $360 \pm 50$  ppbv). The average CO for the remainder of the data was  $141 \pm 40$  ppbv. Of the enhanced CO observations, only 6 minutes corresponded to in-cloud sampling. In-flight video, however, shows the remainder of the enhanced CO to be located both above and below clouds. Thus data collected in cloudy regions may be associated with enhanced trace gases independent of whether the data is specifically within clouds.

### 3. Approach

[9] The above examples provide interesting anecdotal evidence of trace gas enhancements in and around clouds, but it is also desirable to pursue a semiquantitative assessment of the degree to which trace gas distributions vary with local cloudiness. Here, this assessment is pursued through a filtering of the observations from the two aircraft into relevant subsets for comparison. Differences in the statistical distributions of these subsets will then be assessed to identify effects of cloudiness on a regional scale.

[10] Combined data available from both aircraft encompass 188 hours of flight time (93 hours for the P-3B and 95 hours for the DC-8). Actual data coverage, however, varies for a given measurement depending on sampling frequency and integration time. For instance, CO is continuously measured and offers 175 hours of data, whereas NMHC grab samples provide only 96 hours of data. By combining data from the two aircraft, more robust statistics can be achieved. This is most easily justified for measurements which had a common investigator on both aircraft

(e.g., CO, O<sub>3</sub>, and NMHCs). These measurements in particular showed exceptional agreement during several airborne intercomparisons that were flown during TRACE-P [Eisele *et al.*, 2003]. Combining the aircraft data in this analysis is in keeping with the goal of these intercomparisons, which was to show that data collected from the two aircraft could be treated as a single, integrated data set. Other measurements had different investigators on each aircraft, but in most cases, intercomparisons showed good agreement. Still other measurements were only on a single aircraft. These measurements have been included in this analysis, but they necessarily offer less conclusive results. Specific measurement details are available in the TRACE-P overview [Jacob *et al.*, 2003].

[11] The first step in filtering the data involves identifying periods of cloud penetration by each aircraft. This can be achieved through in situ sampling of cloud water or aerosol. How to filter the remaining clear air data for impacts from clouds above or below the aircraft is less straightforward, but is done here by evaluating perturbations to the local (or in situ) radiation field by clouds. This requires radiative transfer modeling, which necessarily limits the analysis to daylight observations with a solar zenith angle less than 85°. This analysis also excludes data from transit flights and focuses on data collected along the Asian Pacific Rim over the western, North Pacific east of 160°E.

#### 3.1. Identification of In-Cloud Data

[12] For the DC-8, potential cloud penetrations were diagnosed through FSSP (forward scattering spectrometer probe) measurements of 10–20  $\mu\text{m}$  particles. When these

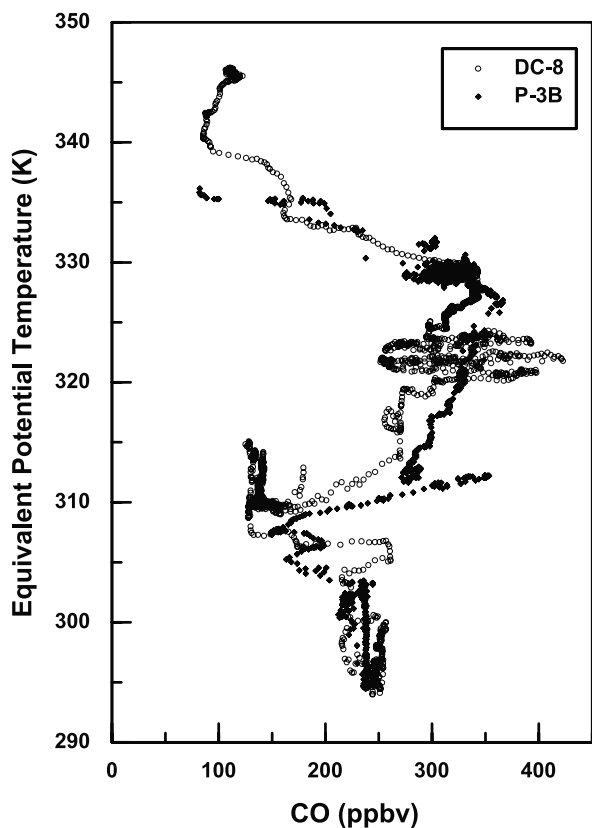


**Figure 3.** Vertical profile of CO through frontal clouds in coordinates of equivalent potential temperature.

measurements surpassed a threshold volume of  $2000 \mu\text{m}^3/\text{cm}^3$ , the data was flagged as a cloud penetration. Volumes of  $800\text{--}2000 \mu\text{m}^3/\text{cm}^3$  were flagged as “intermediate” which included fog, high-altitude cirrus, and thin patches within denser surrounding cloud. In-flight video for the DC-8 was scanned to provide a visual verification of these cloud encounters. For the purposes of this analysis, both cloud and intermediate data are considered to be “in-cloud” data. Cloud penetrations for the P-3B aircraft were identified through Gerber probe measurements of liquid water content. Observations greater than  $0.001 \text{ g}/\text{m}^3$  (or  $1000 \mu\text{m}^3/\text{cm}^3$ ) were treated as in-cloud data. Visual verification using P-3B in-flight video was not extensive, but was spot checked to establish confidence in the Gerber probe data. Combining the in-cloud data for the two aircraft, the frequency of in-cloud sampling during TRACE-P was determined to be just under 10%.

### 3.2. Segregation of Clear Air Data Based on Variability in $j\text{NO}_2$

[13] Further filtering of the remaining data to identify data in cloudy regions but not physically within clouds (i.e., above, below, and between clouds) was based on perturbations to the local radiation field as a proxy for local cloudiness. These perturbations were diagnosed through the use of filter radiometer measurements of the  $\text{NO}_2$  photolysis frequency,  $j\text{NO}_2$ . These measured values for  $j\text{NO}_2$  were compared with values for clear-sky conditions based on radiative transfer calculations. The Tropospheric

Ultraviolet-Visible (TUV) model version 4.1 was used to calculate  $j\text{NO}_2$  along the aircraft flight tracks for all periods with solar zenith angles less than  $85^\circ$ . TUV has been previously described by *Madronich and Flocke* [1999]. For these calculations, TUV was implemented with an eight-stream discrete ordinates scheme radiation solver. Standard model conditions consisted of cloud-free skies, vertical profiles of air,  $\text{O}_3$ , and temperature from the United States Standard Atmosphere (USSA) 1976 and a wavelength independent surface albedo of 10% for ocean and albedo of 5% for the few portions of TRACE-P flights over land. The TOMS  $\text{O}_3$  column data was bilinearly interpolated at the latitude and longitude of the aircraft flight path. This interpolated TOMS  $\text{O}_3$  column was used to scale the standard TUV ozone profile (the annual mean from the U.S. Standard Atmosphere (1976) for  $45^\circ\text{N}$ ) to the measured value. The OPAC Maritime Tropical aerosol profile from *Hess et al.* [1998] has a total aerosol optical depth of 0.056 at 550 nm and a 2 km boundary layer. This Maritime Tropical boundary layer has a single scattering albedo of 0.998 and an asymmetry parameter ( $g$ ) of 0.774 (both at 550 nm) and represents a relatively clean background aerosol condition. For additional details concerning these calculations, see *Lefer et al.* [2003].

[14] By taking the ratio of measured-to-calculated  $j\text{NO}_2$ , the perturbation with respect to clear-sky conditions can be estimated. This ratio will be referred to as the “cloud correction factor” or CCF and has been used in past GTE campaigns to correct other unmeasured  $j$  values for local cloud conditions [*Davis et al.*, 1993; *Crawford et al.*, 1996, 1997; *Jacob et al.*, 1996; *Schultz et al.*, 1999; *Olson et al.*, 2001].

[15] Figure 4a shows the cumulative distribution of the CCF for both in-cloud and clear air data with solar zenith angles less than  $85^\circ$ . For the in-cloud data, the cumulative distribution of the CCF exhibits a nearly uniform slope. This reflects the gradual transition from radiation enhancements in cloud tops to strong attenuation at the bottom of clouds [*Madronich*, 1987]. For the clear air data, the cumulative distribution of the CCF exhibits a central region of modest, relatively constant slope bounded by two regions of rapidly changing slope. Figure 4b shows this slope, along with the clear air cumulative distribution.

[16] Changes in the slope of the cumulative distribution provide a rationale for segregating the data into three groups. These data groups are given the designations low-CCF, mid-CCF, and high-CCF which are also annotated on Figure 4b. The regions of rapidly changing slope represent radiative conditions typically found below clouds (low-CCF) and above clouds (high-CCF). These low-CCF and high-CCF data comprise the lower and upper 20% of the cumulative distribution and represent significant departures from clear-sky conditions. When combined, the cloudy data (i.e., in-cloud, low-CCF, and high-CCF) comprise 46% of the total TRACE-P data set.

[17] The central or mid-CCF data represent radiative conditions approximating clear-sky. The mid-CCF data are characterized by a relatively small slope and CCF values near unity (i.e., 0.78–1.09). The fact that the mid-CCF data are not centered on unity is an indication that there is some bias ( $\sim 10\%$ ) between measured and modeled clear-sky  $j\text{NO}_2$ . This bias is discussed in more detail by *Lefer et al.*

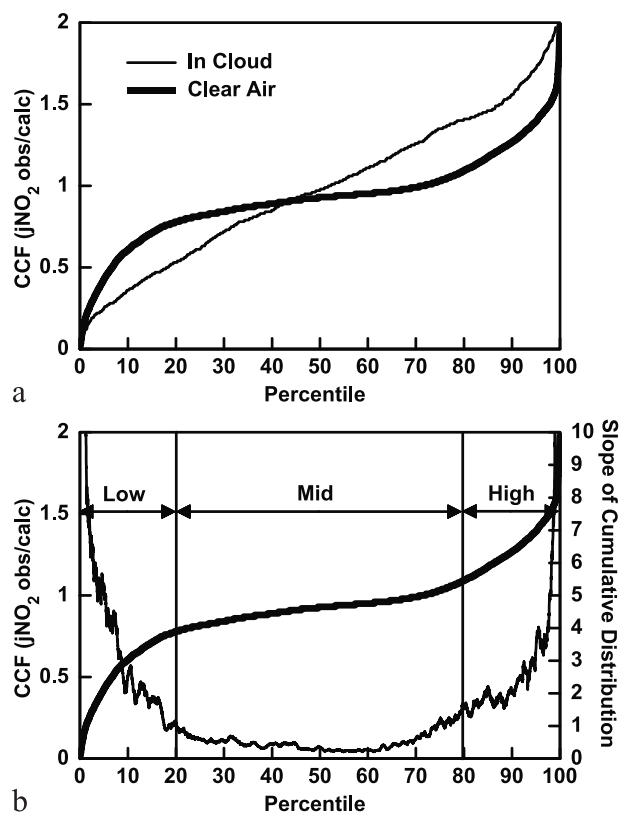


**Figure 4.** (a) Cumulative distributions of the CCF for in-cloud and clear air data and (b) cumulative distribution of the CCF for clear air data and the slope of the distribution. Low-, mid-, and high-CCF data groups are annotated.

[2003]; however, it is not material to this analysis since the segregation of data is based on the variability in  $j\text{NO}_2$ , not the absolute magnitude.

[18] The main strength of the CCF is that it provides an objective measure for segregating the data. At the same time, it must be noted that the CCF has several shortcomings. It does not provide any insight on cloud type, cloud amount, cloud proximity, or cloud history; rather it provides a measure of the degree to which the local radiation field is perturbed by clouds. Since this analysis seeks to examine potential impacts on remote sensing and photochemistry, a diagnostic based on the local radiation field seems appropriate.

[19] Also recognize that it is possible that competing cloud effects within some cloudy regions might result in a CCF near unity. As a result, it is reasonable to expect that some cloudy data falls in the mid-CCF range of data. Conversely, however, it is not reasonable to expect cloud-free conditions to fall into the low-CCF or high-CCF categories. This uncertainty in the segregation of data leads to a more conservative estimate for the differences in trace gases between cloud-free and cloudy regions.

### 3.3. Geographic Distribution of Data

[20] Having identified these data groups, it is important to ensure that there are no significant geographic biases in the cloudy versus the clear-sky data. The spatial distribution of each data group is shown in Figures 5a–5d. The

geographic center mass for each group is shown in Figure 5e. While there are differences in the distribution of each data group, no large differences in proximity to Pacific Rim sources is evident. The largest separation exists between the low-CCF and high-CCF data. A possible explanation for this separation relates to the generally increasing height of frontal clouds with proximity to the low-pressure center of midlatitude cyclones. During TRACE-P, these low-pressure centers were typically located well to the north of the flight tracks [Fuelberg *et al.*, 2003]. As a result, one might expect the probability of flight above clouds (i.e., high-CCF data) to be greater to the south, while flight beneath clouds (i.e., low-CCF data) would likely increase in frequency toward the low-pressure centers to the north. When combining the three cloudy data groups into a single group, the geographic center mass for the cloudy and clear data differ by only one degree in latitude with no significant longitude bias. While latitudinal gradients in trace gases must be acknowledged, data from each group span the full range of latitudes sampled. Sensitivity of these results to the average latitude differences between groups appears to be small but will be addressed in the discussion of results.

[21] In order to make a meaningful comparison, these data groups must finally be binned over discrete altitude

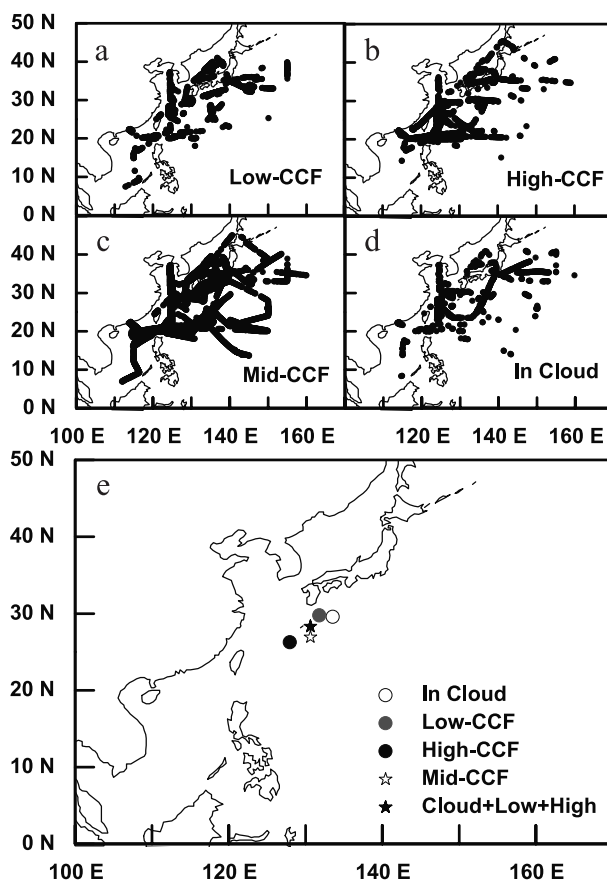


**Figure 5.** Geographic distributions for (a–d) each data group and (e) their geographic center mass.

**Table 1.** Fractional Contribution From Each Data Group for 1 km Altitude Bins<sup>a</sup>

Altitude, km	In Cloud	Low-CCF	Mid-CCF	High-CCF
0–1	0.06 (21)	0.58 (26)	0.35 (24)	0.01 <sup>b</sup> (2)
1–2	0.22 (22)	0.16 (20)	0.51 (26)	0.11 (14)
2–3	0.11 (17)	0.12 (13)	0.59 (26)	0.18 (19)
3–4	0.08 (15)	0.08 (13)	0.58 (26)	0.26 (18)
4–5	0.09 (14)	0.06 (9)	0.61 (26)	0.24 (22)
5–6	0.06 (11)	0.03 <sup>b</sup> (6)	0.64 (24)	0.27 (19)
6–7	0.06 (6)	0.01 <sup>b</sup> (2)	0.67 (17)	0.26 (15)
7–8	0.12 (5)	0.01 <sup>b</sup> (1)	0.56 (13)	0.31 (11)
8–9	0.06 (3)	0.0 <sup>b</sup>	0.65 (12)	0.29 (9)
9–10	0.11 (6)	0.0 <sup>b</sup>	0.64 (12)	0.25 (11)
10–11	0.14 (4)	0.0 <sup>b</sup>	0.59 (10)	0.27 (8)
11–12	0.0 <sup>b</sup>	0.0 <sup>b</sup>	0.77 (5)	0.23 <sup>c</sup> (1)

<sup>a</sup>Number of flights contributing data are given in parentheses.

<sup>b</sup>Data for these bins are not statistically significant.

<sup>c</sup>Data for this bin are not robust since only one flight contributes data.

ranges. This removes any potential for biases in the comparison due to the natural vertical gradient exhibited by most atmospheric trace gases. Table 1 shows the contribution of each data group for 1 km altitude increments. As expected, low-CCF data that tend to be below clouds contribute most heavily in the lower altitudes, and high-CCF data that are most commonly associated with data above clouds do not contribute significantly to the boundary layer data. For statistical robustness, data groups were required to contribute at least 5% to the flight time for a

given altitude with more than two flights contributing data in order to be considered in this analysis.

## 4. Results

### 4.1. Distributions for Selected Species

[22] Figure 6 shows the distributions of CO and ozone sampled along the Asian Pacific Rim during TRACE-P for the four data groups. The distribution of CO shows several interesting features. The most obvious of these features relates to the enhancement of CO for in-cloud data in the upper troposphere above 4 km. In the lower free troposphere between 1 and 5 km, distinct enhancements in CO relative to mid-CCF data exist not only for the in-cloud data, but also for low-CCF and high-CCF data. It is at these lower tropospheric altitudes that the impact of springtime outflow from the Asian Pacific Rim to the North Pacific is most pronounced [Crawford *et al.*, 1997; Talbot *et al.*, 1997; Blake *et al.*, 1997]. In most cases, the median CO for the mid-CCF data is less than the 25th percentile value for the other data groups. Also note that in-cloud data do not stand out from low-CCF and high-CCF data in the lower troposphere below 4 km, reinforcing the idea that frontal lifting of emissions need not be contained within clouds, but will likely be in a region of general cloudiness. In the lowest kilometer, there are no clear differences between groups. This may reflect that outflow at this altitude does not require frontal lifting. On

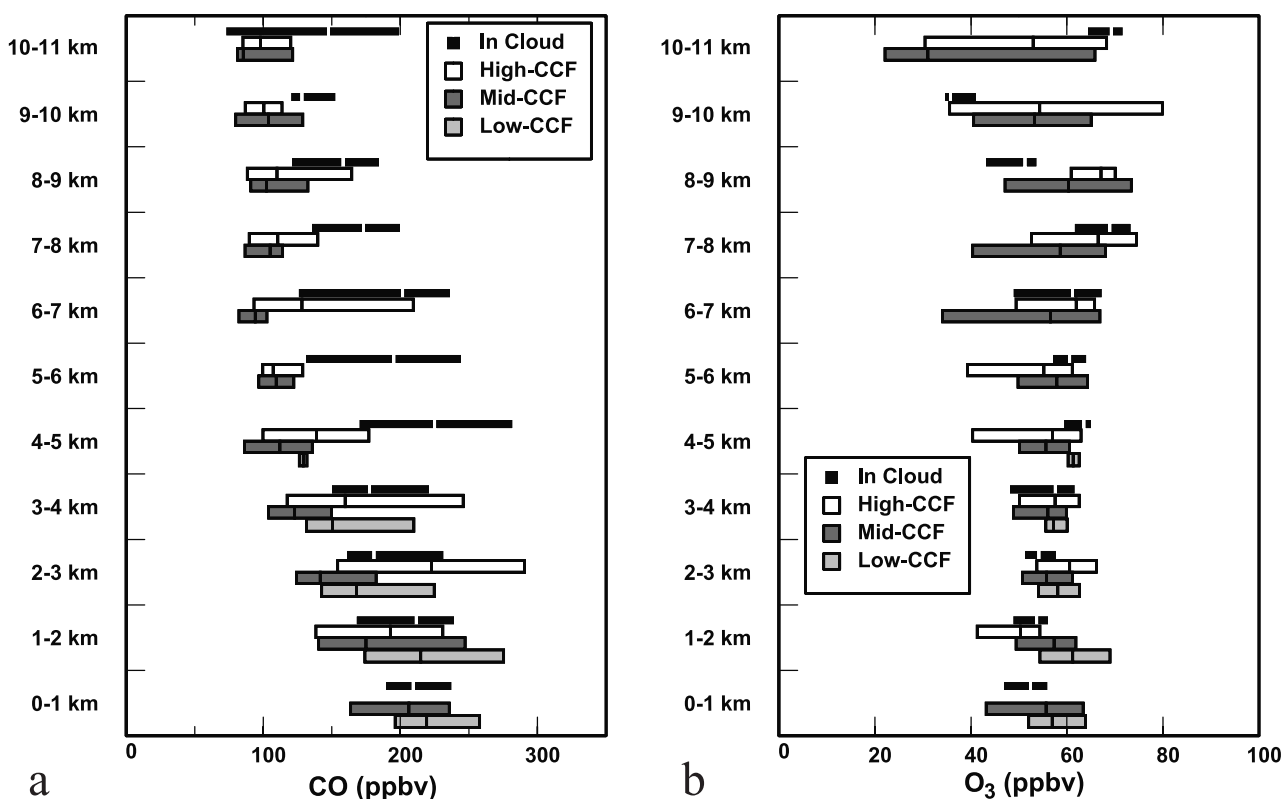


**Figure 6.** Vertical distributions for (a) CO and (b) O<sub>3</sub> for each data group. Center lines indicate median values, and boxes encompass the inner quartiles.

balance, these data strongly suggest that cloudy regions of the western, North Pacific tend to have higher CO mixing ratios.

[23] The distribution of ozone in Figure 6b offers an important contrast to that of CO. In this case, the data demonstrate no compelling tendency between groups. It is important to note that ozone showed less variability than CO observations during TRACE-P, and while ozone is expected to be associated with polluted outflow to the extent that it is photochemically produced, ozone generally showed poor correlation to CO during TRACE-P. Factors contributing to this poor correlation include variations in ozone production efficiency based on source emission characteristics, air mass age, and the influence of stratosphere-troposphere exchange. These competing influences appear to preclude any significant statistical differences in the ozone distribution related to local cloudiness.

[24] Extending the analysis to nonmethane hydrocarbons (NMHCs), Figures 7a–7d show distributions for ethane, propane, n-butane, and i-pentane. These NMHCs have similar sources, but span a wide range of atmospheric lifetimes. As was observed in the CO distribution, each NMHC exhibits a distinct enhancement for in-cloud data in the upper free troposphere above 5 km. In the 1–5 km range, however, there are important differences. Ethane is enhanced for the in-cloud and low-CCF data, while high-CCF ethane is roughly equal to the mid-CCF observations. For propane, n-butane, and i-pentane, enhancements for low-CCF data are even more pronounced, and high-CCF data are depressed relative to mid-CCF data. It is tempting to invoke photochemistry as an explanation for the difference in high-CCF and low-CCF behavior, especially for the shorter-lived NMHCs; however, the lack of enhancement in ethane for the high-CCF data is surprising given that its lifetime (about 2 months in the lower troposphere) is comparable to that of CO. High-CCF enhancements in CO versus the lack of enhancement in ethane would seem to indicate differences in emission sources for the low-CCF and high-CCF data.

[25] While the details of Asian emission sources are highly complex, the most basic distinction that can be drawn is to differentiate between sources from urban/industrial activity and biomass burning. For the TRACE-P data set, the most useful tracers for this purpose are  $C_2Cl_4$  (urban/industrial) and  $CH_3Cl$  (biomass burning) [Blake *et al.*, 1996, 1997, 2003]. While  $C_2Cl_4$  is rather specific, interpretation of  $CH_3Cl$  is complicated by emissions from heavy use of biofuels in Asia [Streets *et al.*, 2003].  $CH_3Cl$  also has an oceanic source roughly equivalent to that associated with biomass burning, however, the integrated source is broadly distributed whereas the biomass burning source is spatially concentrated [Keene *et al.*, 1999]. As a result, it is expected that the ambient variability in  $CH_3Cl$  is largely driven by biomass burning sources. Figure 8 shows distributions for  $C_2Cl_4$  and  $CH_3Cl$ .  $C_2Cl_4$  data in the 1–5 km range tends to be enhanced for low-CCF data and depressed for high-CCF data relative to the mid-CCF data, similar to the behavior of the NMHC data.  $CH_3Cl$  data are enhanced in both the low-CCF and high-CCF data of 1–5 km, but enhancements are much more pronounced for the high-CCF data, especially between 2 and 5 km. These differences between the low-CCF and high-CCF data sug-

gest a prevalence of urban/industrial emissions in the low-CCF data and biomass burning emissions in the high-CCF data.

[26] The consistency between this observation and the differences in NMHCs can be evaluated through the emissions inventories produced for TRACE-P [Streets *et al.*, 2003]. On the basis of these emission inventories, the emission ratio of  $C_2H_6/CO$  (ppbv/pptv) was  $\sim 10$  for both biomass burning and anthropogenic sources. This would seem to be at odds with the enhancements of CO in both the low-CCF and high-CCF data, while ethane was enhanced only for low-CCF data. More consistent with the observed differences between high-CCF and low-CCF data, the emission ratio for propane,  $C_3H_8/CO$ , was two times lower for biomass burning than for anthropogenic sources. For butane and pentane, emission ratios for biomass burning were more than an order of magnitude lower than for anthropogenic emissions.

[27] In trying to reconcile the behavior of ethane, it is important to look into the available information regarding the relative emission of  $C_2H_6$  and CO from biomass burning. The TRACE-P emissions inventory indicates that the biomass burning emissions were dominated by tropical forest burning. Streets *et al.* [2003] indicate that biomass burning emission factors were taken from Andreae and Merlet [2001]. Consulting Andreae and Merlet's [2001] Table 1, the emission of  $C_2H_6$  from tropical forest is assigned a rather large uncertainty with potential emissions ranging from 0.5 to 1.9 g/kg matter burned. Compared to  $104 \pm 20$  g/kg for CO, the true emissions ratio could lie anywhere between 5 and 20. Measurements in biomass burning plumes in the Southern Hemisphere result in ratios between 5.2 and 8.5 [Blake *et al.*, 1996; Ferek *et al.*, 1998]. These values would be more consistent with the ethane trends observed in TRACE-P.

## 4.2. Photochemical Impacts

[28] The potential differences in emissions sources for NMHCs present a complication in using them to assess differences in photochemistry induced by clouds. A more direct approach would be to examine observed OH concentrations. Given the large diurnal variation in OH, these observations must be examined over a range of solar zenith angles. In Figure 9, the distribution of 1–5 km OH has been binned over the solar zenith angle range observed during TRACE-P. The enhanced radiation environment of the high-CCF data stands out across all solar zenith angles with significantly higher OH concentrations. Conversely, the low-CCF data have the lowest OH concentrations for all bins except the 25–35° range. Interpretation of the in-cloud OH data is complicated by the wide range of possible radiative impacts [Madronich, 1987; Weber *et al.*, 2001] as well as the possibility of uptake in cloud droplets [Mauldin *et al.*, 1998; Frost *et al.*, 1999].

[29] Recognizing that variables other than UV intensity play an important role in determining OH (e.g., water vapor, ozone, NO), the coarse assessment presented in Figure 9 strongly supports the notion that the largest impact on OH occurs above clouds with the enhancement of OH. Much of the expected depression of OH below clouds appears to be offset by other factors. Cloud impacts on photochemistry

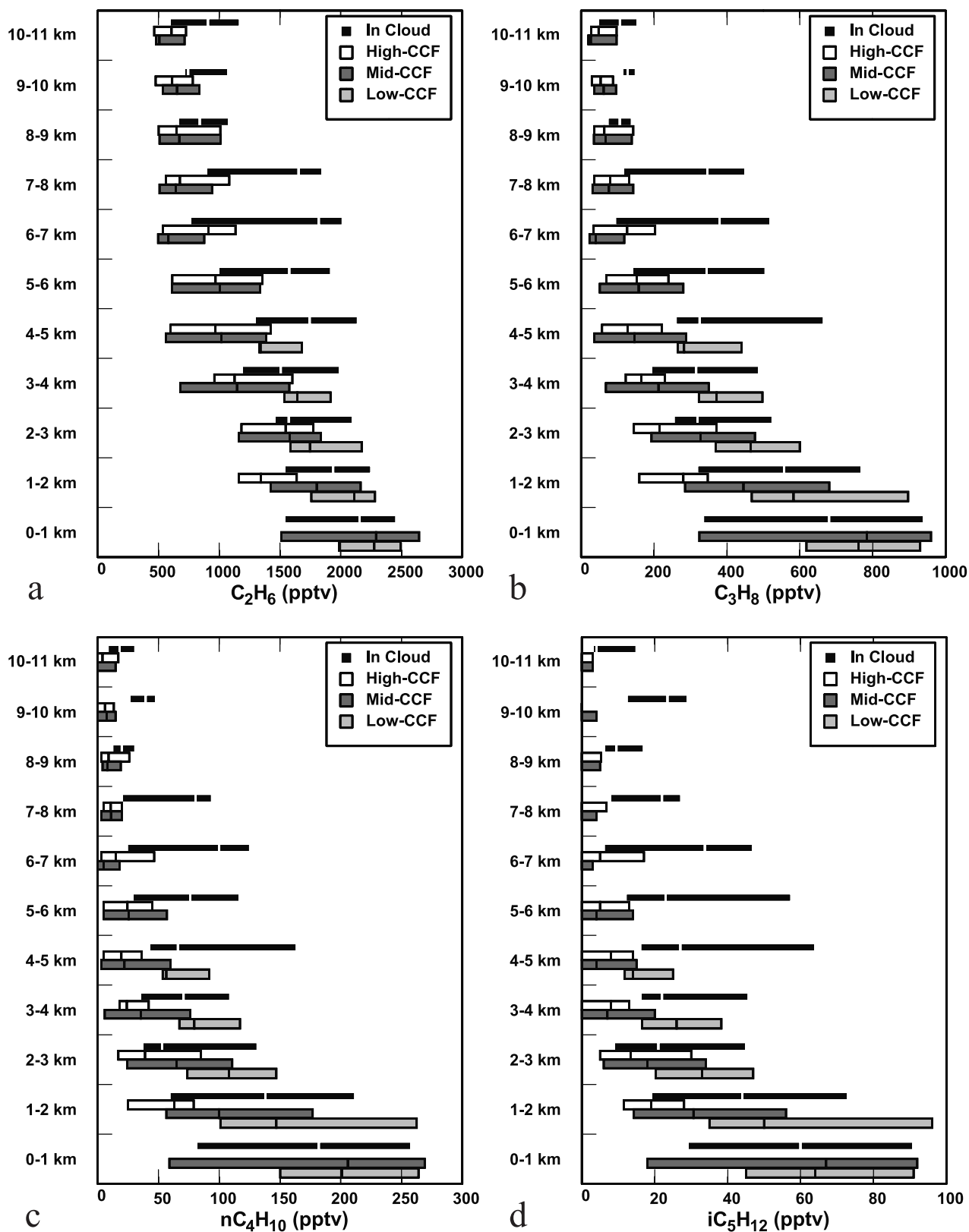
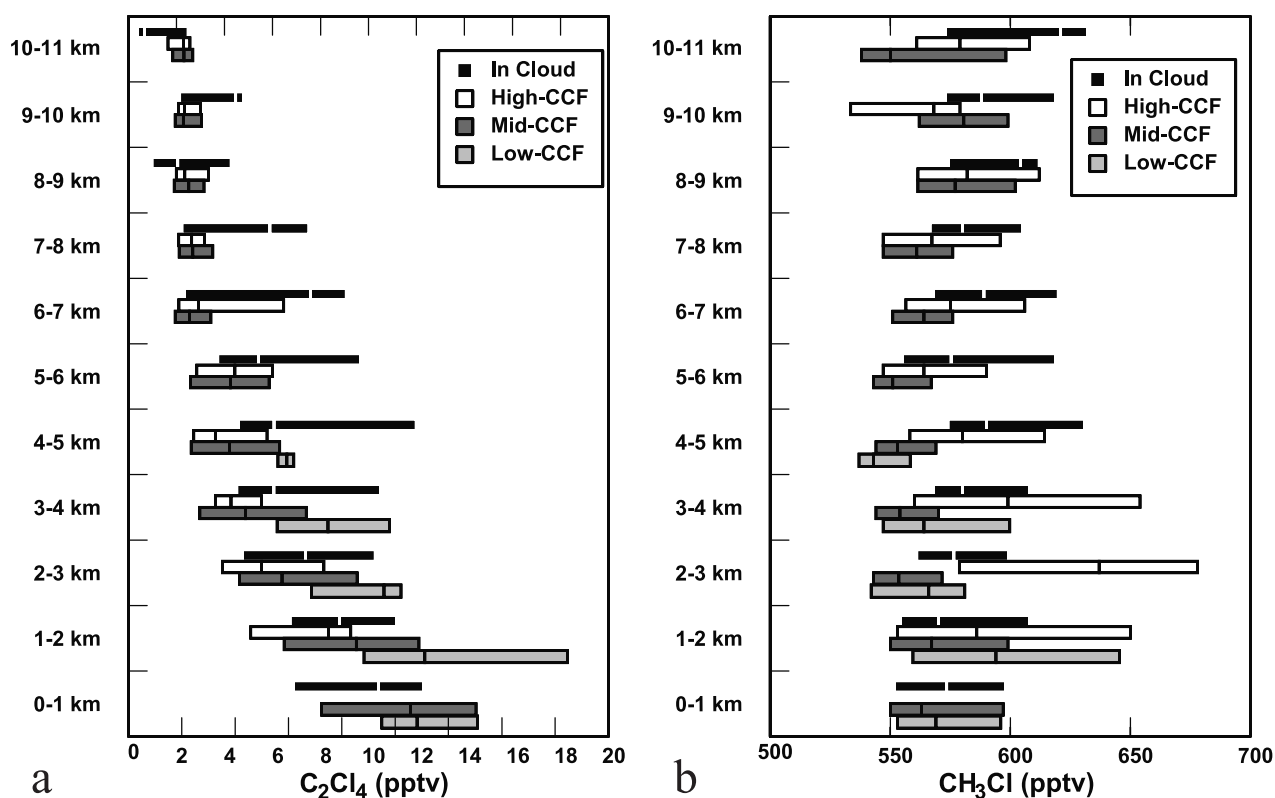


Figure 7. Vertical distributions for (a) ethane, (b) propane, (c) n-butane, and (d) i-pentane for each data group. Center lines indicate median values, and boxes encompass the inner quartiles.



**Figure 8.** Vertical distributions for (a) perchloroethene and (b) methyl chloride for each data group. Center lines indicate median values, and boxes encompass the inner quartiles.

during TRACE-P are examined in much more detail by *Lefer et al.* [2003] and *Tang et al.* [2003].

#### 4.3. Statistics for the Lower Free Troposphere (1–5 km)

[30] Statistics for a wide variety of chemical species are summarized in Table 2 for the lower free troposphere. As mentioned earlier, most of the Asian outflow takes place at these altitudes. These altitudes also experience comparable amounts of low-CCF, high-CCF, and in-cloud data (see Table 1).

[31] In comparing median values for each data group, several patterns emerge. Along with CO, there are numerous tracers for which the in-cloud data have the highest value and the mid-CCF data have the lowest value. These species include the long-lived tracers CO<sub>2</sub>, CH<sub>4</sub>, OCS, and CFCs. This group also includes some shorter-lived combustion products, C<sub>2</sub>H<sub>2</sub> and C<sub>6</sub>H<sub>6</sub>. These tracers are also greater for the low-CCF relative to the high-CCF data. As a tracer of convection, CH<sub>3</sub>I is also maximized in the in-cloud data. Low-CCF and high-CCF data are also significantly enhanced relative to the mid-CCF data, reinforcing the view that these data groups are associated with shallow, frontally induced lifting.

[32] Another group of tracers are maximized for the low-CCF data and minimized for high-CCF data, these include the alkanes as well as C<sub>2</sub>Cl<sub>4</sub> which are preferentially derived from fossil fuel and urban/industrial sources. On the other hand, biomass burning tracers methyl chloride and acetonitrile represent a set of species which are maximized for the high-CCF data.

[33] Reactive nitrogen species show maximum values for low-CCF data and minimum values for mid-CCF data. Reactive nitrogen also shows interesting differences in partitioning. For the low-CCF data, HNO<sub>3</sub> and PAN make similar contributions to NO<sub>y</sub>. The high-CCF data show a

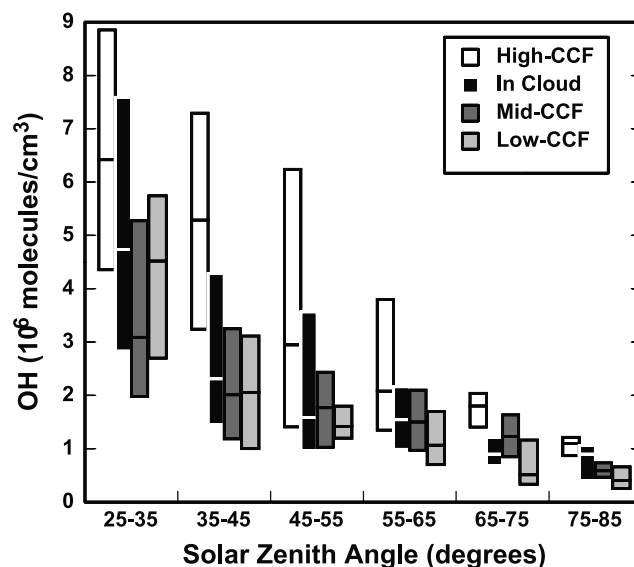


**Figure 9.** Solar zenith angle distributions of measured OH for 1–5 km altitude for each data group. Center lines indicate median values, and boxes encompass the inner quartiles.

**Table 2.** Median Observed Values From Each Data Group for 1–5 km Altitude<sup>a</sup>

	Mid-CCF	Low-CCF	High-CCF	In-Cloud
Altitude, km	3.0	2.5	3.1	2.4
CO, ppbv	(135)	176	163	<b>198</b>
O <sub>3</sub> , ppbv	56	<b>59</b>	57	(55)
NO <sub>x</sub> <sup>b</sup> , pptv	(39)	<b>79</b>	65	68
HNO <sub>3</sub> <sup>c</sup> , pptv	(163)	<b>240</b>	226	175
PAN <sup>c</sup> , pptv	(166)	<b>281</b>	176	243
NO <sub>y</sub> <sup>d</sup> , pptv	(462)	<b>690</b>	535	587
C <sub>2</sub> H <sub>6</sub> , pptv	1426	<b>1822</b>	(1263)	1744
C <sub>3</sub> H <sub>8</sub> , pptv	290	<b>488</b>	(176)	398
n-C <sub>4</sub> H <sub>10</sub> , pptv	57	<b>112</b>	(26)	89
i-C <sub>5</sub> H <sub>12</sub> , pptv	15	<b>36</b>	(9)	28
C <sub>2</sub> Cl <sub>4</sub> , pptv	6.1	<b>10.3</b>	(4.6)	9.1
SO <sub>2</sub> <sup>e</sup> , pptv	80	<b>241</b>	(66)	104
CH <sub>3</sub> Cl, pptv	(556)	568	<b>600</b>	578
CH <sub>3</sub> CN, pptv	123	(116)	<b>168</b>	118
OCS, pptv	(503)	523	513	<b>535</b>
CH <sub>4</sub> , ppbv	(1797)	1817	1814	<b>1829</b>
CO <sub>2</sub> , ppmv	(373.6)	375.1	373.7	<b>375.3</b>
C <sub>6</sub> H <sub>6</sub> , pptv	(58)	117	81	<b>132</b>
C <sub>2</sub> H <sub>2</sub> , ptv	(323)	523	397	<b>595</b>
F-11, pptv	(260)	261	261	<b>262</b>
H-1211, pptv	(4.28)	4.36	4.31	<b>4.41</b>
CH <sub>3</sub> I, pptv	(0.17)	0.28	0.29	<b>0.44</b>

<sup>a</sup>Maximum values bold, and minimum values in parentheses.

<sup>b</sup>Based on calculated NO<sub>2</sub>.

<sup>c</sup>Measured by different investigators on each aircraft.

<sup>d</sup>Measured on P-3B only.

<sup>e</sup>P-3B data only with volcanic plume from flight 17 removed.

lower relative PAN component, possibly related to the lower ethane concentrations. In-cloud data show a lower relative HNO<sub>3</sub> contribution, most likely a sign of cloud scavenging. Other signs of cloud scavenging can be seen in the numbers for SO<sub>2</sub> which are enhanced for low-CCF data by more than a factor of two over all other groups.

[34] Given the observed differences in OH (Figure 9) and the short-lifetime of NO<sub>x</sub>, it is somewhat surprising that there is no compelling evidence for enhanced NO<sub>x</sub> loss in the high-CCF data.

#### 4.4. Statistics for the Upper Free Troposphere (5–11 km)

[35] Statistics for a wide variety of chemical species are summarized in Table 3 for the upper free troposphere. Here the pattern that emerges is rather consistent across species in that almost all of the tracers are maximized for the in-cloud data. Even for the exceptions where high-CCF data are largest, values are not significantly greater than in-cloud values. These results suggest that convection into the upper free troposphere is more closely related to the presence of clouds since there is a much stronger tendency for enhanced emissions to exist within cloud. This is consistent with the picture that frontal passages influence the lower troposphere through large-scale, shallow lifting, while the upper tropospheric influence is dominated by localized deep convection triggered by the front. Nevertheless, high-CCF data still exceed mid-CCF values, although by much smaller amounts.

[36] Although total NO<sub>y</sub> measurements are not available at these altitudes, data for NO<sub>x</sub>, HNO<sub>3</sub>, and PAN show interesting differences in NO<sub>y</sub> partitioning. The increased fraction of PAN for the in-cloud data is almost a factor of 2

greater than for the high-CCF or mid-CCF data. At the same time, each category has comparable levels of NO<sub>x</sub> and HNO<sub>3</sub>. While the increase in PAN may reflect direct vertical transport, it could also be the result of transporting PAN precursors to colder altitudes where PAN is more thermally stable. This change in the thermal equilibrium would sequester more NO<sub>x</sub> in the form of PAN possibly contributing to the lack of NO<sub>x</sub> enhancement for in-cloud data. Meanwhile, the lack of an enhancement in HNO<sub>3</sub> for in-cloud data might reflect cloud scavenging during vertical transport.

## 5. Implications for Remote Sensing

[37] The value of obtaining information on tropospheric chemistry from satellites is unquestioned. Satellite observations of only a few key species stand to provide important contextual information critical to the interpretation of more detailed in situ observations at the surface and from aircraft. Satellite observations can also provide critical information to global and regional models for model testing and/or assimilation to improve our understanding of tropospheric chemistry. At the same time, satellite observations of tropospheric chemistry face numerous difficulties in that they are restricted by clouds and are also challenged by the presence of aerosols, water vapor, and stratospheric ozone [Singh and Jacob, 2000]. Having demonstrated the differences in trace gas concentrations between cloudy and clear conditions during TRACE-P, clouds would seem to present not only a loss of information, but should also impose a bias on observations from satellite. Given the TRACE-P data, it is of interest to estimate what the magnitude of this bias might be.

**Table 3.** Median Observed Values From Each Data Group for 5–11 km Altitude<sup>a</sup>

	Mid-CCF	High-CCF	In-Cloud
Altitude	7.4	7.8	8.2
CO	(101)	108	<b>155</b>
O <sub>3</sub>	(57)	59	<b>61</b>
NO <sub>x</sub> <sup>b</sup>	(43)	<b>50</b>	49
HNO <sub>3</sub> <sup>c</sup>	(117)	127	<b>130</b>
PAN <sup>c</sup>	(122)	141	<b>265</b>
NO <sub>y</sub> <sup>d</sup>	–	–	–
C <sub>2</sub> H <sub>6</sub>	(647)	704	<b>1100</b>
C <sub>3</sub> H <sub>8</sub>	(65)	74	<b>141</b>
n-C <sub>4</sub> H <sub>10</sub>	(7)	10	<b>35</b>
i-C <sub>5</sub> H <sub>12</sub>	LOD	LOD	<b>17</b>
C <sub>2</sub> Cl <sub>4</sub>	(2.55)	2.60	<b>5.26</b>
SO <sub>2</sub> <sup>d</sup>	–	–	–
CH <sub>3</sub> Cl	(563)	575	<b>589</b>
CH <sub>3</sub> CN	(152)	<b>168</b>	161
OCS	(490)	492	<b>514</b>
CH <sub>4</sub>	(1762)	1766	<b>1783</b>
CO <sub>2</sub>	(371.8)	372.0	<b>373.8</b>
C <sub>6</sub> H <sub>6</sub>	(14)	22	<b>75</b>
C <sub>2</sub> H <sub>2</sub>	(134)	168	<b>347</b>
F-11	(259)	259	<b>260</b>
H-1211	(4.18)	4.18	<b>4.40</b>
CH <sub>3</sub> I	(0.06)	0.08	<b>0.29</b>

<sup>a</sup>Maximum values bold, and minimum values in parentheses.

<sup>b</sup>Based on calculated NO<sub>2</sub>.

<sup>c</sup>Measured by different investigators on each aircraft.

<sup>d</sup>P-3B data only; insufficient data above 5 km.

**Table 4.** Observed CO Enhancements for Cloudy Conditions<sup>a</sup>

	Mid-CCF	Cloudy <sup>b</sup>	Enhancement, %
<i>1–5 km Altitude</i>			
Median	135	178	32
25th percentile	110	136	24
75th percentile	171	246	44
Mean	156	198	27
Median, <20°N	101	111	10
Median, 20–30°N	129	182	41
Median, >30°N	145	190	31
<i>5–11 km Altitude</i>			
Median	101	116	15
25th percentile	83	97	17
75th percentile	118	150	27
Mean	107	132	23
Median, <20°N	92	109	18
Median, 20–30°N	93	105	13
Median, >30°N	114	130	14

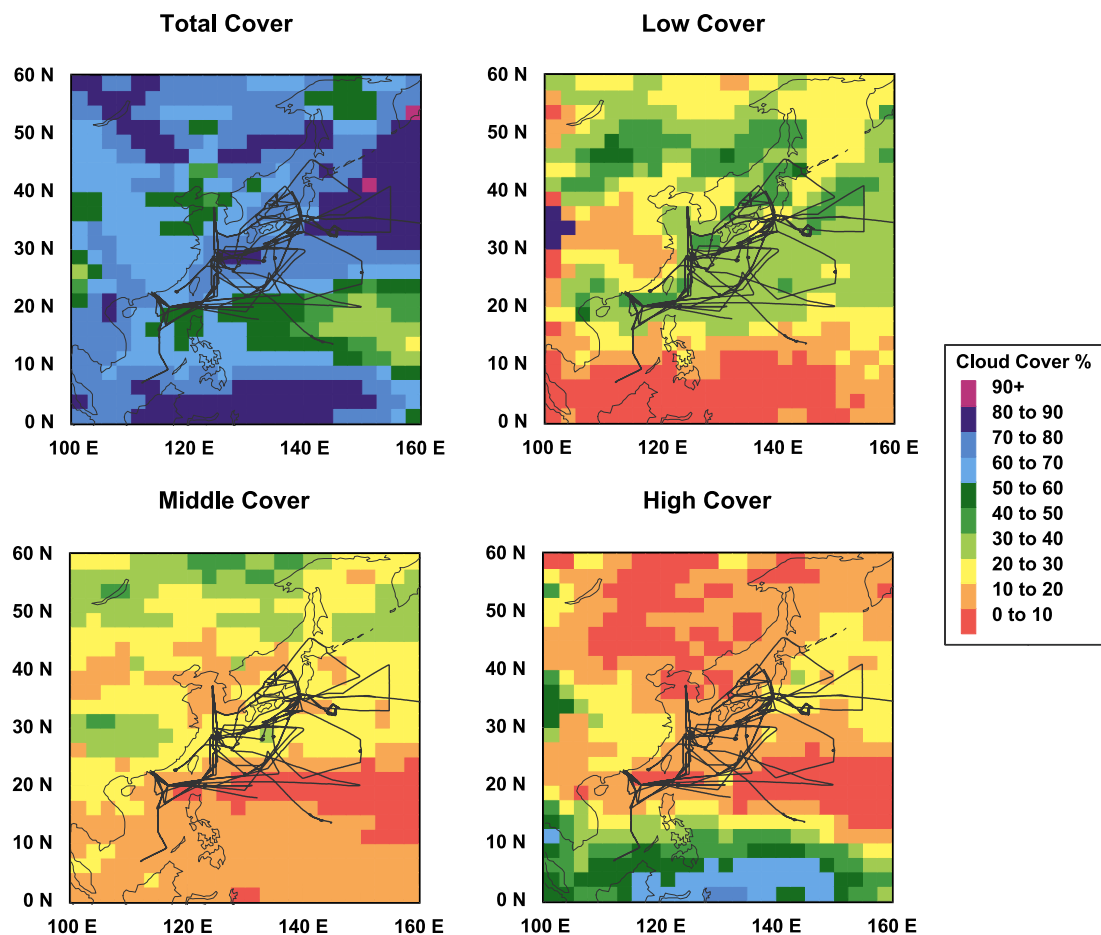
<sup>a</sup>In units of ppbv.<sup>b</sup>In-cloud, low-CCF, and high-CCF data combined.

[38] To assess the overall bias between cloudy and clear regions, the low-CCF, high-CCF, and in-cloud data can be combined into a single “cloudy” data group. When considering data in the 1–5 km range, the median CO mixing ratio for this cloudy data is 178 pptv versus 135 pptv for the mid-CCF data, an enhancement of 32%. For the 5–11 km

range, cloudy data have a median CO of 116 ppbv. This value exceeds the mid-CCF value of 101 ppbv by 15%. Recall that while upper tropospheric enhancements in CO can be quite large, they are mainly limited to in-cloud data which represents a relatively small portion of the observations at these altitudes. Nevertheless, these enhancements represent nontrivial impacts on the CO column abundance. As a result, it is not unreasonable to expect that spatially and temporally averaged, space-based observations over the western, North Pacific could underestimate total CO.

[39] The robustness of these estimated enhancements are examined in Table 4 by looking at other percentile and mean statistics. Data are also segregated by latitude. The various statistics provide strong support that the overall median statistics are reasonable estimates for the enhancement of CO in cloudy regions. The only statistic that stands out is the median enhancement for 1–5 km data <20°N. In this case, the smaller 10% enhancement is consistent with the weak influence of frontal outflow on the lower troposphere at these tropical latitudes.

[40] In assessing cloudy versus clear data, the question arises concerning the actual amount of cloud cover over the TRACE-P region. On the basis of the filtering of aircraft data, 46% of the TRACE-P data was identified as cloudy data. At various altitudes, the percentage of cloudy data fell mostly in the 30–50% range (see Table 1). Figure 10 shows cloud cover statistics for the Asian Pacific Rim during

**Figure 10.** ISCCP cloud cover statistics over the TRACE-P domain for March 2001.

March, 2001 from ISCCP (International Satellite Cloud Climatology Project) [Rossow and Schiffer, 1999]. This coincides nicely with the TRACE-P period as the two aircraft reached the Pacific Rim on 4 March (Hong Kong) and departed on 3 April (Yokota AFB, Japan). The ISCCP data indicate that the level of cloudiness over the TRACE-P region may be even greater than that inferred from the airborne measurements. On the basis of the TRACE-P flight tracks, total cloud cover in the range of 70–80% should have been expected. This cloud cover was primarily low cloud (30–40%) with lesser amounts of middle and high cloud (20–30% and 10–20%, respectively).

[41] While ISCCP cloud cover statistics do have a slight bias (+0.05) compared to surface observations from both land and ocean [Rossow and Schiffer, 1999], this bias is too small to explain the 20–30% lower cloud cover inferred from the TRACE-P flight data. Several factors may contribute to this difference. First, the threshold for identifying clouds in this work based on  $j\text{NO}_2$  is not directly comparable to ISCCP and may not be as sensitive an indicator. Also, as mentioned earlier, in situ determinations of  $j\text{NO}_2$  in complex cloud fields should allow for some portion of cloudy data to fall in the mid-CCF range due to competing cloud influences. Another factor contributing to this difference is a bias toward clear skies in the deployment of the aircraft. This is most relevant to the DC-8 platform which often sought clear skies for the purposes of performing satellite validation profiles for the MOPITT instrument on NASA's Terra satellite. The presence of remote sensing equipment (i.e., UV-DIAL) onboard the DC-8 also created a preference for clear skies.

## 6. Conclusions

[42] During the TRACE-P mission, outflow of Asian emissions from the Pacific Rim to the western, North Pacific was sampled by NASA's DC-8 and P-3B aircraft. Outflow was found to be mediated primarily by the passage of frontal disturbances. On several occasions, enhanced CO mixing ratios were observed in and around frontal clouds.

[43] A more detailed analysis of trace gas distributions was conducted by separating the data into four groups: in-cloud, low-CCF, mid-CCF and high-CCF. The in-cloud data represented periods of cloud penetration by the aircraft, while the other three groups were based on perturbations to the local radiation field diagnosed using measurements and clear-sky calculations of  $j\text{NO}_2$ . The low-CCF and high-CCF groups represented data from cloudy regions where  $j\text{NO}_2$  was significantly lower (low-CCF) or higher (high-CCF) than the expected clear-sky value. The mid-CCF data represented mostly clear conditions where  $j\text{NO}_2$  was at or near the expected clear-sky value.

[44] Distributions for CO revealed significant enhancement for all cloud associated groups compared to the mid-CCF data. Above 5 km, in-cloud data especially stood out from the other groups, while low-CCF and high-CCF values showed greatest enhancements in the 1–5 km range. Observations in the lowest kilometer revealed no clear differences between groups; however, outflow at the surface does not depend on frontal lifting. Distributions for ozone revealed no clear differences between the four data groups suggesting that other influences (e.g., lower ambient variability,

variations in production efficiency, air mass age, and stratosphere-troposphere exchange) might disrupt any relationship between local cloudiness and ozone mixing ratios. Similar to CO, most tracers of anthropogenic origin showed enhancement in the cloud associated data relative to the mid-CCF group. Limited evidence for cloud scavenging was seen in data for  $\text{HNO}_3$  and  $\text{SO}_2$ .

[45] Measurements of OH were consistent with the expectation that photochemical oxidation should be enhanced for high-CCF data and depressed for low-CCF conditions. Despite these differences in OH, no clear evidence of enhanced or depressed photochemistry could be extracted from data for short-lived species. This is most likely due to insufficient exposure time to the cloud perturbed photochemical environment which is most likely only about one or maybe two days at the most. Nevertheless, the lack of a trend in  $\text{NO}_x$  data was surprising given its short lifetime.

[46] Overall estimates of CO enhancement for cloudy versus clear data were 32% for 1–5 km (178 versus 135 ppbv) and 15% for 5–11 km (116 versus 101 ppbv). These results indicate that cloudy regions may represent much more than missing data to spaced-based observations of tropospheric chemical constituents. For instance, TRACE-P data would suggest that a satellite-derived, average CO column abundance for the western, North Pacific during spring would almost certainly underestimate the true CO abundance if based only on clear-sky observations. It is reasonable to expect that other marine regions downstream of continental sources might also exhibit a relationship between cloudiness and trace gas abundance, e.g., North American outflow of emissions to the North Atlantic and outflow of biomass burning emissions from Africa and South America to the South Atlantic. On the other hand, remote regions such as the Tropical and South Pacific would most likely not exhibit any clear relationship between clouds and trace gas distributions. To better understand the conditions under which trace gas distributions might be related to local cloudiness, this type of analysis needs to be applied to other airborne data sets.

[47] **Acknowledgments.** This work was supported by the NASA Tropospheric Chemistry Program. The authors would also like to thank the pilots and crew of the NASA's DC-8 and P-3B aircraft for their efforts in support of the TRACE-P flights. ISCCP data used in this paper were obtained from <http://isccp.giss.nasa.gov/>.

## References

- Andreae, M. O., and P. Merlet, Emission of trace gases and aerosols from biomass burning, *Global Biogeochem. Cycles*, **15**, 955–966, 2001.
- Bey, I., D. J. Jacob, J. A. Logan, and R. M. Yantosca, Asian chemical outflow to the Pacific: Origins, pathways, and budgets, *J. Geophys. Res.*, **106**, 23,097–23,114, 2001.
- Blake, N. J., D. R. Blake, B. C. Sive, T.-Y. Chen, F. S. Rowland, J. E. Collins Jr., G. W. Sachse, and B. E. Anderson, Biomass burning emissions and vertical distribution of atmospheric methyl halides and other reduced carbon gases in the South Atlantic region, *J. Geophys. Res.*, **101**, 24,151–24,164, 1996.
- Blake, N. J., D. R. Blake, T.-Y. Chen, J. E. Collins Jr., G. W. Sachse, B. E. Anderson, and F. S. Rowland, Distribution and seasonality of selected hydrocarbons and halocarbons over the western Pacific Basin during PEM-West A and PEM-West B, *J. Geophys. Res.*, **102**, 28,315–28,331, 1997.
- Blake, N., et al., NMHCs and halocarbons in Asian continental outflow during TRACE-P: Comparison to PEM-West B, *J. Geophys. Res.*, **108**(D20), 8806, doi:10.1029/2002JD003367, 2003.
- Cooper, O. R., J. L. Moody, D. D. Parrish, M. Trainer, T. B. Ryerson, J. S. Holloway, G. Hübler, F. C. Fehsenfeld, and M. J. Evans, Trace gas

- composition of midlatitude cyclones over the western North Atlantic Ocean: A conceptual model, *J. Geophys. Res.*, 107(D7), 4056, doi:10.1029/2001JD000901, 2002a.
- Cooper, O. R., J. L. Moody, D. D. Parrish, M. Trainer, J. S. Holloway, G. Hübler, F. C. Fehsenfeld, and A. Stohl, Trace gas composition of midlatitude cyclones over the western North Atlantic Ocean: A seasonal comparison of O<sub>3</sub> and CO, *J. Geophys. Res.*, 107(D7), 4057, doi:10.1029/2001JD000902, 2002b.
- Crawford, J., et al., Photostationary state analysis of the NO<sub>2</sub>-NO system based on airborne observations from the western and central North Pacific, *J. Geophys. Res.*, 101, 2053–2072, 1996.
- Crawford, J., et al., An assessment of ozone photochemistry in the extratropical western North Pacific: Impact of continental outflow during late winter/early spring, *J. Geophys. Res.*, 102, 28,469–28,487, 1997.
- Davis, D. D., et al., A photostationary state analysis of the NO<sub>2</sub>-NO system based on airborne observations from the subtropical/tropical North and South Atlantic, *J. Geophys. Res.*, 98, 23,501–23,523, 1993.
- Dickerson, R. R., et al., Thunderstorms: An important mechanism in the transport of air pollutants, *Science*, 235, 460–465, 1987.
- Eisele, F., et al., Summary of measurement intercomparisons during TRACE-P, *J. Geophys. Res.*, 108(D20), 8791, doi:10.1029/2002JD003167, 2003.
- Ferek, R. J., J. S. Reid, P. V. Hobbs, D. R. Blake, and C. Liousse, Emission factors of hydrocarbons, halocarbons, trace gases, and particles from biomass burning in Brazil, *J. Geophys. Res.*, 103, 32,107–32,118, 1998.
- Frost, G. J., et al., Photochemical modeling of OH levels during the First Aerosol Characterization Experiment (ACE 1), *J. Geophys. Res.*, 104, 16,041–16,052, 1999.
- Fuehlberg, H. E., C. Kiley, J. R. Hannan, D. J. Westberg, M. A. Avery, and R. E. Newell, Meteorological conditions and transport pathways during the transport and chemical evolution over the Pacific (TRACE-P) experiment, *J. Geophys. Res.*, 108(D20), 8782, doi:10.1029/2002JD003092, 2003.
- Hess, M., P. Koepke, and I. Schult, Optical properties of aerosols and clouds: The software package OPAC, *Bull. Am. Meteorol. Soc.*, 79(5), 831–844, 1998.
- Huntreiser, H., H. Schlager, C. Feigl, and H. Höller, Transport and production of NO<sub>x</sub> in electrified thunderstorms: Survey of previous studies and new observations at midlatitudes, *J. Geophys. Res.*, 103, 28,247–28,264, 1998.
- Jacob, D. J., et al., Origin of ozone and NO<sub>x</sub> in the tropical troposphere: A photochemical analysis of aircraft observations over the South Atlantic basin, *J. Geophys. Res.*, 101, 24,235–24,250, 1996.
- Jacob, D. J., J. Crawford, M. M. Kleb, V. S. Connors, R. J. Bendura, J. L. Raper, G. W. Sachse, J. Gille, L. Emmons, and J. C. Heald, Transport and Chemical Evolution over the Pacific (TRACE-P) mission: Design, execution, and first results, *J. Geophys. Res.*, 108(D20), 9000, doi:10.1029/2002JD003276, 2003.
- Junker, W., et al., Actinic radiation and photolysis processes in the lower troposphere: Effect of clouds and aerosols, *J. Atmos. Chem.*, 42, 413–441, 2002.
- Kaneyasu, N., K. Takeuchi, M. Hayashi, S.-I. Fujita, I. Uno, and H. Sasaki, Outflow patterns of pollutants from east Asia to the north Pacific in the winter monsoon, *J. Geophys. Res.*, 105, 17,361–17,377, 2000.
- Keene, W. C., et al., Composite global emissions of reactive chlorine from anthropogenic and natural sources: Reactive Chlorine Emissions Inventory, *J. Geophys. Res.*, 104, 8429–8440, 1999.
- Lefer, B., R. E. Shetter, S. Hall, J. Crawford, and J. Olson, Impact of clouds and aerosols on photolysis frequencies and photochemistry during TRACE-P: 1. Analysis using radiative transfer and photochemical box models, *J. Geophys. Res.*, 108(D21), 8821, doi:10.1029/2002JD003171, in press, 2003.
- Liu, H., D. J. Jacob, I. Bey, R. Yantosca, B. N. Duncan, and G. W. Sachse, Transport pathways for Asian pollution outflow over the Pacific: Interannual and seasonal variations, *J. Geophys. Res.*, 108(D20), 8786, doi:10.1029/2002JD003102, 2003.
- Madronich, S., Photodissociation in the atmosphere: 1. Actinic flux and the effects of ground reflections and clouds, *J. Geophys. Res.*, 92, 9740–9752, 1987.
- Madronich, S., and S. Flocke, The role of solar radiation in atmospheric chemistry, in *Environmental Photochemistry*, edited by P. Boule, pp. 1–26, Springer-Verlag, New York, 1999.
- Mauldin, R. L., III, G. J. Frost, G. Chen, D. J. Tanner, A. S. H. Prevot, D. D. Davis, and F. L. Eisele, OH measurements during the First Aerosol Characterization Experiment (ACE 1), Observations and model comparisons, *J. Geophys. Res.*, 103, 16,713–16,729, 1998.
- McNeal, R. J., J. P. Mugler Jr., R. C. Harriss, and J. M. Hoell Jr., NASA Global Tropospheric Experiment, *Eos Trans. AGU*, 64, 561–562, 1983.
- Olson, J. R., et al., Seasonal differences in the photochemistry of the South Pacific: A comparison of observations and model results from PEM-Tropics A and B, *J. Geophys. Res.*, 106, 32,749–32,766, 2001.
- Pickering, K. E., et al., Convective transport of biomass burning emissions over Brazil during TRACE-A, *J. Geophys. Res.*, 101, 23,993–24,012, 1996.
- Rossov, W. B., and R. A. Schiffer, Advances in understanding clouds from ISCCP, *Bull. Am. Meteorol. Soc.*, 80, 2261–2287, 1999.
- Schultz, M. G., et al., On the origin of tropospheric ozone and NO<sub>x</sub> over the tropical South Pacific, *J. Geophys. Res.*, 104, 5829–5843, 1999.
- Singh, H. B., and D. J. Jacob, Future directions: Satellite observations of tropospheric chemistry, *Atmos. Environ.*, 34, 4399–4401, 2000.
- Streets, D., et al., An inventory of gaseous and primary aerosol emissions in Asia in the year 2000, *J. Geophys. Res.*, 108(D21), 8809, doi:10.1029/2002JD003093, in press, 2003.
- Talbot, R. W., et al., Chemical characteristics of continental outflow from Asia to the troposphere over the western Pacific Ocean during February–March 1994: Results from PEM-West B, *J. Geophys. Res.*, 102, 28,255–28,274, 1997.
- Tang, Y., et al., Impacts of aerosols and clouds on photolysis frequencies and photochemistry during TRACE-P: 2. Three-dimensional study using a regional chemical transport model, *J. Geophys. Res.*, 108(D21), 8822, doi:10.1029/2002JD003100, in press, 2003.
- Thompson, A. M., The effect of clouds on photolysis rates and ozone formation in the unpolluted troposphere, *J. Geophys. Res.*, 89, 1341–1349, 1984.
- Weber, R. J., G. Chen, D. D. Davis, R. L. Mauldin, D. J. Tanner, F. L. Eisele, A. D. Clarke, D. C. Thornton, and A. R. Bandy, Measurements of enhanced H<sub>2</sub>SO<sub>4</sub> and 3–4 nm particles near a frontal cloud during the First Aerosol Characterization Experiment (ACE 1), *J. Geophys. Res.*, 106, 24,107–24,117, 2001.
- Yienger, J. J., et al., The episodic nature of air pollution transport from Asia to North America, *J. Geophys. Res.*, 105, 26,931–26,945, 2000.
- B. Anderson, M. Avery, J. Barrick, G. Chen, J. Crawford, C. Jordan, J. Olson, and G. Sachse, Atmospheric Sciences, MS 483, NASA Langley Research Center, Hampton, VA 23681-0001, USA. (b.e.anderson@larc.nasa.gov; j.d.barrick@larc.nasa.gov; g.chen@larc.nasa.gov; j.h.crawford@larc.nasa.gov; c.e.jordan@larc.nasa.gov; j.o.olson@larc.nasa.gov)
- A. Bandy and D. Thornton, Department of Chemistry, Drexel University, Philadelphia, PA 19104-2875, USA. (alan.bandy@drexel.edu)
- D. Blake, Department of Chemistry, University of California, Irvine, CA 92697, USA. (drblake@uci.edu)
- W. Brune, Department of Meteorology, Pennsylvania State University, 503 Walker Bldg., University Park, PA 16802, USA. (brune@ems.psu.edu)
- A. Clarke, School of Ocean and Earth Science and Technology, University of Hawaii, 1000 Pope Road, Honolulu, HI 96822, USA. (tclarke@soest.hawaii.edu)
- D. Davis, S. Sandolm, and D. Tan, School of Earth and Atmospheric Sciences, Georgia Institute of Technology, Atlanta, GA 30332, USA. (dd16@prism.gatech.edu; dtan@eas.gatech.edu)
- F. Eisele, B. Lefer, F. Flocke, L. Mauldin, and R. Shetter, Atmospheric Chemistry Division, National Center for Atmospheric Research, 1850 Table Mesa Dr., P.O. Box 3000, Boulder, CO 80307-3000, USA. (lefer@ucar.edu; ffil@acd.ucar.edu; shetter@ucar.edu)
- H. Harder and M. Martinez, Atmospheric Chemistry Department, Max Planck Institute for Chemistry, Postfach 3060, D-55020 Mainz, Germany. (harder@mpch-mainz.mpg.de; martinez@mpch-mainz.mpg.de)
- Y. Kondo, Research Center for Advanced Science and Technology, University of Tokyo, 4-6-1 Komaba Meguro-ku, Tokyo, 153-8904, Japan. (kondo@atmos.rcast.u-tokyo.ac.jp)
- H. Singh, NASA Ames Research Center, MS 245 5, 21 Langley Blvd., Moffett Field, CA 94035, USA. (hsingh@mail.arc.nasa.gov)
- R. Talbot, Institute for the Study of Earth, Oceans, and Space, University of New Hampshire, 39 College Road/Morse Hall, Durham, NH 03824-3525, USA. (robert.talbot@unh.edu)
- M. Zondlo, Southwest Sciences Inc., 1570 Pacheco Street, Suite E-11, Santa Fe, NM 87505, USA. (mzondlo@swsciences.com)